Wheaton Journal of
Neurobiology Research

Issue 11, Fall 2018:

R.L. Morris, Editor. Wheaton College, Norton, Massachusetts.

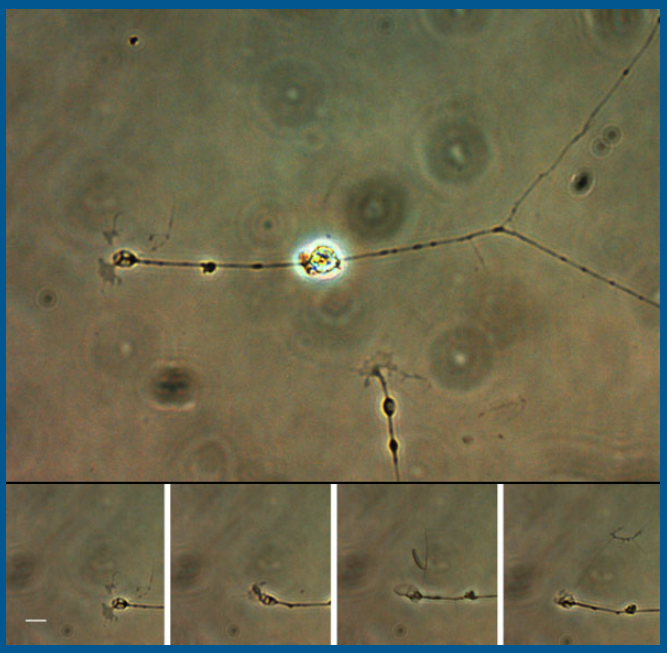

# A preliminary study of mercury (II) chloride in relation to rate of axonal outgrowth in *Gallus gallus* neurons

Meggin Q. Costa

BIO 324 / Neurobiology
Final Research Paper
5 December 2018

# A preliminary study of mercury (II) chloride in relation to outgrowth in *Gallus gallus* neurons

Meggin Q. Costa
Final Research Paper written for
Wheaton Journal of Neurobiology Research
BIO 324 / Neurobiology
Wheaton College, Norton Massachusetts
5 December 2018

## INTRODUCTION

Microtubules are a type of protein filament that contribute to the cytoskeletal framework of cells. These filaments are composed of alternating alpha- and beta-tubulin subunits that are configured in 'head-to-tail' linear arrays (Dent & Gertler, 2003). The arrangement of these tubulin subunits imparts structural polarity to the filament; one end of which is consequently designated as "plus," while the apposed end is designated as "minus." The plus end of the microtubule is subject to cyclic periods of growth and shrinkage that are punctuated by transient pauses (Dent & Gertler, 2003). This collective behavior is intrinsic to the plus end of the microtubule, and is referred to as dynamic instability—a property that is mediated by associated growth-promoting and growth-inhibiting factors (Dent & Gertler, 2003). The ability of microtubules to undergo dynamic rearrangements in response to signaling cues is critical to axonal outgrowth, as these filaments are foundational components of axon shafts, and constitute the central domains of growth cones, which probe the extracellular space (Ertuk, Hellal & Bradke, 2007). Mercury has been implicated as a chemorepellent in this regard (Yen, R., 2006).

Mercury is one of the most toxic heavy metals, and exists in elemental, inorganic, and organic forms; each of which exhibit unique toxicity profiles. Methyl Mercury (MeHg), an organic form of the compound, has been amply studied and is documented to induce neurotoxic effects in the Central Nervous System (CNS) (Broussard, Hammett-Stabler, Winecker & Ropero-Miller, 2002). The most common route of MeHg exposure in humans occurs via fish consumption. Following its absorption into the bloodstream, MeHg achieves systemic circulation by binding to hemoglobin in red blood cells and, to a lesser extent, to sulfhydryl groups present in plasma proteins (Broussard, Hammett-Stabler, Winecker & Ropero-Miller, 2002). Upon crossing the blood brain barrier (BBB), MeHg slowly undergoes demethylation through which free $Hg^{2+}$ ions are produced. These ions are incapable of traversing the BBB and, consequently, are retained within the brain. Mercury ($Hg^{2+}$) is highly lipophilic and is therefore able to readily diffuse across the neuronal plasma membrane and into the cytoplasm of the cell; wherein it is thought to affect large-scale microtubule disassembly by binding to the sulfhydryl groups of tubulin subunits (Broussard, Hammett-Stabler, Winecker & Ropero-Miller, 2002; Lohren et al., 2015).

In the wake of the Industrial and Agricultural Revolutions, a strong correlation was observed between an increase in environmental levels of heavy metals and a pervasive increase in the onset of neurodegenerative disease (Tasneem et al., 2015). Evidence has since emerged

that the pathology of Alzheimer's Disease (AD), a prominent type of neurodegenerative disorder, may be induced or worsened by inorganic mercury exposure (Mutter et al., 2010). Suggestive to this end, mercury-induced microtubule depolymerization has been implicated in cellular damage that manifests as a cessation of neuronal motility and, on a larger scale, macroscopic tissue damage that is consistent with the brain lesions observed in AD patients (Leong *et al*., 2001).

In a study conducted by Leong, Syed & Lorscheider (2001), roughly 77% of *Lymnaea stagnalis* neurons exposed to mercury (II) chloride exhibited growth cone collapse within minutes of treatment. As axonal retraction has been consistently demonstrated as a facet of mercury neurotoxicity, unaffected growth cones observed in this study prompted inquiry as to whether maturational changes in microtubules may have promoted insusceptibility to the effects of mercury exposure (Leong *et al*.,2001; Tasneem, S. *et al*, 2016; Xu, F. *et al.*, 2012). Further, it was hypothesized that developing, less differentiated neurons may be more vulnerable to the effects of mercury than older, more developed neurons (Reuhl *et al*., 1994). The present study seeks to test this hypothesis.

In this study, younger and older *Gallus gallus* neurons were exposed to mercury (II) chloride (100nM). *Gallus gallus* was selected for use as this model organism enabled observation of growth cone dynamics and axonal outgrowth in a vertebrate context. Younger neurons (1-day in culture post-dissection) were utilized to represent less differentiated neurons, and older neurons (4 days in culture post-dissection) were used to represent neurons in which microtubules may have sustained favorable maturational changes. Mercury in the +2-oxidation state was specifically selected for use in order to model $Hg^{2+}$ retention in the brain post-MeHg exposure. Thus, in addition to following up on the study performed by Leong *et al.* (2001), the present study also sought to provide a platform in which to study the microscopic changes that give rise to the macroscopic pathology of neurodegenerative disease. The rate of axonal outgrowth was quantified as a surrogate measure of microtubule polymerization, as this behavior supports, and therefore corresponds to, positive axonal outgrowth.

# MATERIALS AND METHODS

Cell Culture Conditions

Cell culture conditions were cultivated in accord with a published procedure (Morris, R.L. (b), 2018).

Dorsal Root Ganglion Harvest and Culture Allocation

Dissection of 10-day older *Gallus gallus* embryos was executed in accord with a published procedure for the purpose of dorsal root ganglion harvest (Morris, R.L., 2017). The coverslips on which the primary cultures were plated were cleansed and treated following a published protocol (Morris, R.L., 2017). Primary DRG cultures were stored in an incubator (37$^{o}$ C). These procedures were followed for both the younger and older neurons under study. Three primary DRG cultures were utilized within each cohort—one culture per condition. DRG harvest was performed by Professor Robert L. Morris of the Biology Department at Wheaton College in Norton, MA.

Preparation of Mercury ($Hg^{2+}$) Aliquot

A 10 mL aliquot of mercury (II) chloride (13.6 mg/L) was obtained from Professor Janina Benoit of the Chemistry Department at Wheaton College in Norton, MA. This stock solution was stored in a Teflon-stoppered vessel within a refrigerator. Three 5 ml aliquots of

varying concentrations (2,500 nM, 500 nM, and 100 nM) were prepared from the mercury (II) chloride stock solution via serial dilution with Hank's Balanced Salt Solution (HBSS). This was done in collaboration with Anik Mutsuddy, Justin Gallagher, and Sydney LittleJohn. To produce the 2,500 nM aliquot, 1 mL of the mercury (II) chloride stock solution was pipetted into a 10 mL Eppendorf tube. This volume was then raised to 5 mL via the addition of 4 mL of HBSS. The 500 nM aliquot was then produced by pipetting 1 mL of the 2500 nM aliquot into a 10 mL Eppendorf tube. This volume was then raised to 5 mL via the addition of 4 mL of HBSS. To obtain the desired working concentration (100 nM), as determined from the Methods of Leong *et al.* (2001), 1 mL of the 500 nM aliquot was pipetted into a 10 mL Eppendorf tube; into which 4 mL of HBSS was subsequently pipetted. These aliquots, secured upright in a test tube rack, were stored in a refrigerator for the duration of the study.

Experimental Design

Younger neurons were defined as one day post-dissection, and older neurons were defined as four days post-dissection. Three conditions (Control #1, Control #2, and Experimental) were studied within each cohort. Control #1 was defined as neurons plated on coverslips treated with laminin and poly-lysine. This Control was implemented for the purpose of demonstrating neuronal growth within the previously described culture conditions but without the shearing forces in the next control. Control #2 was defined as neurons plated on coverslips treated with laminin and poly-lysine that underwent three washes with HBSS and a subsequent fifteen-minute incubation (37$^{o}$C) in HBSS. This condition was implemented in order to control for the shearing force exerted on the plated neurons during a complete buffer exchange. Controlling for this step is necessary as the described buffer change could disrupt neuronal substrate adhesion, which could potentially impact outgrowth (Yen, 2006). The Experimental condition was defined as neurons plated on coverslips treated with laminin and poly-lysine that underwent three washes with HBSS and a subsequent fifteen-minute incubation (37$^{o}$C) in mercury (II) chloride (100 nM, ~ 2 mL).

HBSS Wash and Mercury ($Hg^{2+}$) Induction

Note that this section is relevant to Control #2 and Experimental conditions within each cohort. Prior to removal of primary DRGs from the 37$^{o}$C incubator, nitrile gloves were adorned and cleansed with 70 % Ethanol. The cultures were then ported carefully from the incubator to an area of bench top that had been previously cleansed with 70 % Ethanol. Materials required for the HBSS wash (and mercury induction in the case of the Experimental condition) were then assembled. These include 5.75-inch Pasteur pipettes, pipette bulbs, one 110 mm petri dish lid for HBSS waste, one 110 mm petri dish lid for collection of withdrawn growth medium, one tissue culture bottle for collection of withdrawn mercury-tainted HBSS, a tissue culture bottle of HBSS, and the 10 mL Eppendorf tube containing mercury (II) chloride (5 mL, 100 nM). The washes were then performed as follows.

In the case of the Control #2 condition, all of the growth medium initially in the 35 mm petri dishes was removed (~ 2 mL). This was done by lifting part of the petri dish off of the lab bench so that the growth medium collected on the side of the dish that remained in contact with the bench top. The tip of a Pasteur pipette was then inserted into this collection; the growth medium was then withdrawn. The withdrawn growth medium was then pipetted into the designated 110 mm petri dish lid. A different Pasteur pipette, designated specifically for use with HBSS, was then used to withdraw HBSS from the stock container. The withdrawn HBSS was

then pipetted into the 35 mm petri dish. The tip of the pipette was directed away from the coverslip and the HBSS was perfused slowly as to minimize shearing force on the cultured DRG. Care was taken to perform washes quickly so as to minimize inducement of cellular stress due to lack of liquid media. The lid of the 35 mm petri dish was then replaced, and the culture was allowed to sit for a period of two minutes post-lid replacement; following which, the lid was once again removed.

All HBSS was then withdrawn from the 35 mm petri dish. HBSS removal followed the same procedure as that previously described for growth medium removal. Withdrawn HBSS was pipetted into the designated 110 mm petri dish lid. A designated pipette was then used to withdraw HBSS from the stock container. The withdrawn HBSS was then pipetted into the 35 mm petri dish following the same procedure of addition previously described. The lid was then replaced and the petri dish was allowed to sit for a period of two minutes. This wash was then performed two additional times. The lid was replaced after the third iteration of this wash. The dish was then ported to the incubator (37$^{o}$C); in which the DRG culture incubated in HBSS for a period of fifteen minutes post-placement. Following the conclusion of this incubation period, the dish was carried back to the lab bench, where the HBSS was removed. Excess growth medium( ~4 mL) was then added to the dish. This was done to mitigate evaporation. The dish was then transferred to the stage of a Nikon TS100 Inverted Routine Microscope for imaging. These steps were performed for the Control #2 condition in both the younger and older neuron cohorts.

In the case of the Experimental condition, the DRG culture underwent triplicate HBSS washes as described above. The culture was then incubated in dilute mercury (II) chloride (100 nM, ~2 mL) for a period of fifteen minutes post-placement within the incubator (37$^{o}$C). Following the conclusion of this incubation period, the dish was returned to the lab bench, where the mercury (II) chloride medium was removed in its entirety. Excess growth medium( ~4 mL) was then added to the dish, which was then transferred to the stage of a Nikon TS100 Inverted Routine Microscope for imaging.

Placement of Culture on Stage of Microscope

The focal length of the 40X objective lens was not satisfied by the distance of the microscope stage above the lens. This was evidenced by an inability to focus at the coverslip layer of the 35 mm petri dish using the 40X objective lens. This level had been previously visualized using the 4X, 10X, and 20X objective lenses. To meet the focal length of the 40X objective lens, the 35 mm petri dish was placed atop two parallel microscope slides that were braced on the stage of a Nikon TS100 Inverted Routine Microscope. Note that the slides were oriented on either side of the 40X objective lens—that is, the slides did not obscure the field of view.

Video-Enhanced Time Lapse Microscopy

A time-lapse sequence of brightfield-transmitted light images was acquired in collaboration with Justin Gallagher for each condition of both the younger and older neuron cohorts using a SPOT idea camera of magnification 0.50X and associated SPOT software (version 4.6). Images were manually acquired via the "Get Image" directive of SPOT software at five-minute intervals for a duration of thirty minutes. During this time, the temperature of the stage of the Nikon TS100 Inverted Routine Microscope was maintained at approximately 37$^{o}$ C. This was accomplished via use of a portable space heater and digital temperature probe. The temperature probe was taped to the stage of the inverted scope, and the space heater was placed

approximately 18 inches from the base of the inverted microscope in order to maintain the desired stage temperature.

A region of interest, defined as containing at least one clearly visible growth cone, was initially identified at 10X magnification using the bifocals of the inverted microscope. Once in focus, the region of interest was displayed on the screen of an Apple Macintosh desktop computer using SPOT software (version 4.6). The region of interest was then mapped at 20X so as to facilitate subsequent location of identified growth cones at 40X magnification. Mapping was performed by taping an 8.5X11 transparent sheet to the screen of the Apple Macintosh computer. The corners of the sheet were aligned with those of the projected image. A black Sharpie marker was then used to trace over the axonal network, as well as any artifact, observed within the region.

The opacity and phase darkness of the growth cones identified in the region of interest were enhanced at 40X magnification by modifying the brightness, gain limit, and gamma settings of the SPOT software. These settings were accessed via the directive, "Show Image Settings" of the SPOT software. The brightness and gamma values chosen varied across conditions within each cohort.

The Control #1 condition of the younger neuron cohort was imaged at a brightness value of 0.35, a gain limit value of 2, and a gamma value of 0.43. The Control #2 condition of this cohort was imaged at a brightness value of 1.00, a gain limit value of 1, and a gamma value of 0.69. The Experimental condition of this cohort was imaged at a brightness value of 1.00, a gain limit value of 1, and a gamma value of 0.58.

The Control #1 Condition of the older neuron cohort was imaged at a brightness value of 0.56, a gain limit value of 1, and gamma value of 0.17. The Control #2 condition of this cohort was imaged at a brightness value of 0.56, a gain limit value of 1, and a gamma value of 0.28. The Experimental condition of this cohort was imaged at a brightness value of 0.51, a gain limit value of 1, and a gamma value of 0.23.

Image Analysis

Image analysis was performed on the Apple Macintosh desktop computer, "Leo" in the Imaging Center for Undergraduate Collaboration (ICUC) at Wheaton College in Norton, Massachusetts. Image sequences were downloaded onto the desktop of this computer and were opened in ImageJ (version 1.52a). The discrete images were then converted to an image stack via the pathway, "Image"→"Stacks"→ "Images to Stack." Note that the "Image" menu was located within the ImageJ taskbar. Once stacked, image type was converted to "8-bit," and the brightness and contrast settings were adjusted to the range, 0-194. This range was selected in accord with perceived visualization quality. Brightness and contrast settings were located via the route, "Image"→ "Adjust"→ "Brightness & Contrast."

The scale of the image stacks was determined by imaging a scale bar (0.1 mm to 0.01 mm) at 40X magnification using the SPOT idea camera of a Nikon TS100 Inverted Routine Microscope. This image was then opened in the ImageJ program installed on the Apple Macintosh desktop computer, "Leo." The line segment tool of the ImageJ software was used to quantify the number of pixels that spanned a known distance of 200 micrometers. This was done by plotting a horizontal line from the right side of the leftmost gradation mark to the right side of the rightmost gradation mark. The distance of the line segment was then measured via the shortcut, "Command"→ "M." This was performed in triplicate. The average of the resulting values (6.586 pixels/micrometer) was considered to be the scale of the images obtained.

Rate of axonal outgrowth was measured via the change in the coordinate location of the centroid of a growth cone within an image stack. The centroid measurement function of ImageJ was located via the pathway, "Analyze"→ "Set Measurements"→ "Centroid." The centroid of a particular growth cone was measured by first outlining the boundaries of the growth cone using the polygon tool located in the ImageJ tools taskbar, and then by selecting the "Measure" function, which was located in the "Analyze" menu. This function was also performed via the shortcut, "Command"→"M."

A growth cone was defined as a phase dark, terminal region of an axon that included both filopodial and lamellipodial protrusions. The beginning of a growth cone was identified visually as a widening of the axon. This 'widening' was subsequently determined to constitute, on average, a 43% increase in uniform axon caliber; the mean value of which was determined to be approximately 1.26 micrometers. The measurements that gave rise to these calculated average values were obtained by measuring one growth cone at four time points within each condition of each cohort. Averages of these data were computed in a Microsoft® Excel® 2016 MSO (16.0.11001.20064) 32-bit spreadsheet.

The boundaries of filopodial and lamellipodial protrusions were distinguished from the background of an image by normalizing the mean gray value (GV) of a protrusion to that of the immediately adjacent background. The mean GVs of these regions were measured using the area tool, which was located in the toolbar menu of the ImageJ software. Normalized values were computed for at least three growth cones within each condition of each cohort. The range of the normalized values was then computed within a Microsoft® Excel® 2016 MSO (16.0.11001.20064) 32-bit spreadsheet. Filopodial and lamellipodial protrusions were subsequently defined as phase dark protrusions whose normalized mean GV was 0.633 to 0.984 gray values below that of the immediately adjacent background.

Centroid measurements were collected in accord with these criteria. Growth cones that fell beyond the image frame were disregarded; as were those that were obscured by artifact. Centroid coordinate data was converted to distance (in pixels) using the distance formula. This distance was subsequently converted to micrometers using image scale (6.586 pixels/micrometer). The distances per growth cone were averaged for each condition within each cohort—that is, one average growth rate value (in micrometers/minute) was obtained per condition within each neuron cohort.

Statistical Analysis

Analysis of Variation (ANOVA) was utilized to test differences between the mean axonal growth rate of neurons subjected to each condition within each cohort. Note that equal variances were assumed within each cohort. Minitab Express software was utilized to perform this analysis.

# RESULTS

Dynamic filopodial and lamellipodial behaviors were observed in each condition of both the younger (1-day in culture post-dissection) and older (4 days in culture post-dissection) neuron cohorts (Figure 1). It is interesting to note that neurons in the Control #2 condition of the younger cohort exhibited a greater average rate of axonal outgrowth (1.230 $\mu$m/min) than those in the Experimental condition of this cohort (1.148 $\mu$m/min). Similarly, neurons in the Control #2 condition of the older cohort exhibited a greater average rate of axonal outgrowth (0.9090

$\mu$m/min) than those in the Experimental condition of this cohort (0.8671 $\mu$m/min). Overall, younger neurons exhibited greater average rates of axonal outgrowth than older neurons (Figure 2). Observed differences, however, are not statistically significant.

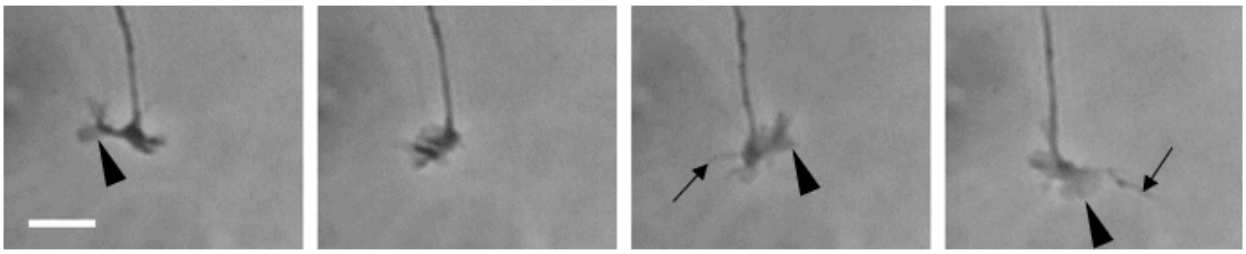

**Figure 1: An image sequence of representative growth cone motility exhibited by neurons within the Experimental condition of the older cohort.** The growth cone activity depicted in this sequence occurred over the span of fifteen minutes. These images were brightness- and contrast-adjusted. Notice the dynamic behavior of filopodial and lamellipodial protrusions. Solid arrow heads indicate lamellipodia and solid arrows indicate filopodia.

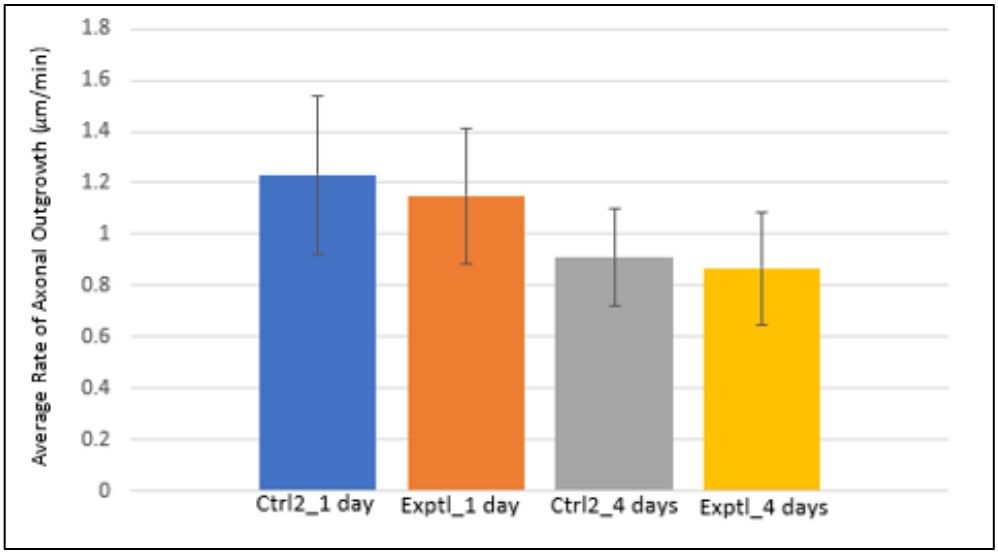


**Figure 2: The average growth rates exhibited by neurons within each condition of both the younger (1 day) and older (4 days) cohorts.** The difference of average growth rates between Ctrl2_1 day and Exptl_1 day are not significant (p=0.6387). The difference of average growth rates between Ctrl2_4 days and Exptl_4 days is not significant (p=0.7879). The difference in average growth rates between the Ctrl2_1 day and Ctrl2_4 days is not significant (p=0.1032). The difference between Exptl_1 day and Exptl_4 days is not significant (p=0.0604). Data were derived from 28 centroid measurements obtained from four discrete growth cones depicted in eight sample images acquired from one trial of the Control #2 condition of the younger neuron cohort. Data were derived from 21 centroid measurements obtained from three discrete growth cones depicted in eight sample images acquired from one trial for the Experimental condition within the older neuron cohort. Data were derived from 21 centroid measurements for three discrete growth cones depicted in eight sample images acquired for one trial of the Control #2 condition of the older neuron cohort. Data were derived from 14 centroid measurements of for two discrete growth cones depicted in eight sample images acquired for one trial for the Experimental condition of the older neuron cohort.

# DISCUSSION AND CONCLUSIONS

Based on existing literature (Leong *et al.*, 2001), it was hypothesized that younger neurons (1-day in culture post-dissection) would exhibit heightened sensitivity to mercury (II) chloride relative to older neurons (4 days in culture post-dissection) as assayed via average axonal outgrowth rate. The results of the current study, however, refute this hypothesis, as the difference in average axonal outgrowth rate between the control and experimental conditions was not significantly different. Moreover, no significant effect of mercury treatment was observed in this study.

These results are surprising as there is a strong consensus that implicates mercury ($Hg^{2+}$) in microtubule depolymerization, which, has been shown to manifest as axonal retraction and a lack of positive outgrowth in neurons (Leong *et al*.,2001; Tasneem, S. *et al*, 2016; Xu, F. *et al.*, 2012). That the concentration of mercury (100 nM) utilized in this study did not perturb axonal outgrowth is particularly puzzling, as this concentration of mercury (II) chloride or less is known to yield robust axonal retraction and cell death in culture (Leong et al. 2001; Tasneem, S. *et al*, 2016; Xu, F. *et al.*, 2012). It is important to note, however, that these studies did not employ *Gallus gallus* neurons. Difference in axonal response to mercury ($Hg^{2+}$), perhaps as a result of variation in microtubule stability, may therefore be species-specific.

One mechanism by which mercury may affect axonal outgrowth might be through an effect on microtubule stability. Microtubule-associated proteins (MAPs), including MAP6 and MAP2, have been implicated in the indirect stabilization of microtubules via the inhibition of proteins that promote microtubule severing or depolymerization (Baas, P *et al.*, 2016). The mechanisms that underlie this stabilization are not well-characterized; however, assuming that the mercury induced in the current study successfully entered the neurons, it is possible that the mercury ions, though not protein, were mitigated via these or similar mechanisms. The potential difference in axonal outgrowth rate observed between the neuron cohorts of the present study may also be attributable whence, as the microtubules of adult and developing neurons differ in stability properties (Baas, P. *et al.*, 2016).

The unperturbed axonal outgrowth observed in the present study may also be due to inactivation of the N-methyl-D-aspartate (NMDA) receptor. Recent studies have correlated mercury neurotoxicity with an overstimulation of the NMDA receptor, as inhibition of this receptor is known to prevent mercury-induced cytoskeletal disruption (Xu, F. *et al.*, 2012). Activation of this receptor via phosphorylation of its cytosolic domain has been associated with reactive oxygen species (ROS) (Gau, X. *et al.*, 2007), which arise in association with mercury-induced oxidative stress. It is possible, therefore, that mitigation of mercury ions via the previously proposed MAPS mechanism may have prevented this ion from inducing an intracellular ROS influx, which may have prevented activation of the NMDA receptor; thereby inhibiting cytoskeletal degeneration.

It is interesting to note that neither perturbation of growth cone morphology nor perturbation of filopodial and lamellipodial behaviors were observed, as depicted in Figure 1. This phenomenon is consistent with existing literature (Leong et al., 2001; Xu, F. *et al.*, 2012). Quantification of these behaviors was beyond the scope of the present study, but would constitute an interesting area of future research. Given that filopodia and lamellipodia are actin-supported extensions of plasma membrane, a plausible hypothesis might be that inorganic

mercury ($Hg^{2+}$) lacks affinity for actin subunits, and is therefore incapable of inducing microfilament depolymerization.

To refine the present study, a mercury (II) dose curve should be performed in order to assess the effects of different concentrations of mercury (II) chloride on axonal outgrowth in *Gallus gallus* neurons. Existing literature suggests that the degree of mercury-induced axonal retraction is duration- and concentration-dependent (Teixeira, F. et al., 2018). In addition, axonal outgrowth rates for neurons in the experimental and control conditions of each cohort should be quantified prior to mercury exposure, as this would provide a baseline average rate of axonal outgrowth for a particular condition; from which the degree of any observed rate variation could be subsequently quantified. It would also be beneficial to implement fluorescent staining of tubulin subunits, as this technique would provide a direct measure of tubulin abundance and organization. This information would more effectively lend insight into the mechanism(s) by which inorganic mercury ($Hg^{2+}$) induces neurotoxicity.

# REFERENCES


Askew, A. (2013). The Effects of Mercury Polymerization in Axons of Gallus gallus neurons. Wheaton College Journal of Neurobiology.

Baas, P. W., Rao, A. N., Matamoros, A. J., & Leo, L. (2016). Stability properties of neuronal microtubules. Cytoskeleton, 73(9), 442-460. doi:10.1002/cm.21286

Broussard, L. A., PhD, DABCC, FACB, Hammett-Stabler, C. A., PhD, DABCC, FACB, Winecker, R. E., PhD, & Ropero-Miller, J. D., PhD. (august 2002). The Toxicology of Mercury. Laboratory Medicine, 33(8).

Dent, E. W., & Gertler, F. B. (2003). Cytoskeletal Dynamics and Transport in Growth Cone Motility and Axon Guidance. Neuron, 40(2), 209-227. doi:10.1016/s0896-6 273(03)00633-0

Ertuk, A., Hellal, F., & Bradke, F. (2007). Disorganized Microtubules Underlie the Formation of Retraction Bulbs and the Failure of Axonal Regeneration. Society for Neuroscience.

Gao, X., Kim, H. K., Chung, J. M., & Chung, K. (2007). Reactive oxygen species (ROS) are involved in enhancement of NMDA-receptor phosphorylation in animal models of pain. *Pain, 131*(3), 262-271. doi:10.1016/j.pain.2007.01.011

Leong, C. C., Syed, N. I., & Lorscheider, F. L. (2001). Retrograde degeneration of neurite membrane structural integrity of nerve growth cones following in vitro exposure to mercury. Neuroreport,12(4), 733-737. doi:10.1097/00001756-200103260-00024

Lohren, H., Blagojevic, L., Fitkau, R., Ebert, F., Schildknecht, S., Leist, M., & Schwerdtle, T. (2015). Toxicity of organic and inorganic mercury species in differentiated human neurons and human astrocytes. Journal of Trace Elements in Medicine and Biology, 32, 200-208. doi:10.1016/j.jtemb.2015.06.008

Morris, R.L. (2017). Primary Culture of Chick Embryonic Peripheral Neurons 1: DISSECTION

Morris, R.L. (b) (2018). Neurobiology/ Bio 324 – Problem Set 1

Mutter, J., Curth, A., Naumann, J., Deth, R., & Walach, H. (2010). Does Inorganic Mercury Play a Role in Alzheimers Disease? A Systematic Review and an Integrated Molecular Mechanism. Journal of Alzheimers Disease, 22(2), 357-374. doi:10.3233/jad-2010-100705

Tasneem, S., Farrell, K., Lee, M., & Kothapalli, C. R. (2016). Sensitivity of neural stem cell survival, differentiation and neurite outgrowth within 3D hydrogels to environmental heavy metals. Toxicology Letters, 242, 9-22. doi:10.1016/j.toxlet.2015.11.021

Teixeira, F. B., Oliveira, A. C., Leão, L. K., Fagundes, N. C., Fernandes, R. M., Fernandes, L. M., . . . Lima, R. R. (2018). Exposure to Inorganic Mercury Causes Oxidative Stress, Cell Death, and Functional Deficits in the Motor Cortex. Frontiers in Molecular Neuroscience, 11. doi:10.3389/fnmol.2018.00125

Xu, F., Farkas, S., Kortbeek, S., Zhang, F., Chen, L., Zamponi, G. W., & Syed, N. I. (2012). Mercury-induced toxicity of rat cortical neurons is mediated through N-methyl-D-Aspartate receptors. Molecular Brain, 5(1), 30. doi:10.1186/1756-6606-5-30

Yen, R. (2006). Growth Cone retraction rate in time and on substrata when subjected to sublethal doses of mercury. Wheaton College Journal of Neurobiology.